






Article

Energy Cane Ash: Property Assessment for Its Valorization in Sustainable Cementing Systems

Gabriela Pitolli Lyra ¹, Lisiane Brichi ², Josefa Roselló ³, María Victoria Borrachero ⁴, Lourdes Soriano ^{4,*}, Jordi Payá ⁴ and João Adriano Rossignolo ¹

¹ Department of Biosystems Engineering, Faculdade de Zootecnia e Engenharia de Alimentos, Universidade de São Paulo (USP), Pirassununga 13635-900, SP, Brazil; gabriela.lyra@usp.br (G.P.L.); rossignolo@usp.br (J.A.R.)

² Escola Superior de Agricultura Luiz de Queiroz, Universidade de São Paulo (USP), Piracicaba 13418-900, SP, Brazil; lisianebrichi@gmail.com

³ Department of Agroforestry Ecosystems, Universitat Politècnica de València (UPV), 46022 València, Spain; jrosello@upvnet.upv.es

⁴ Institute of Concrete Science and Technology (ICITECH), Universitat Politècnica de València (UPV), 46022 València, Spain; vborrachero@cst.upv.es (M.V.B.); jjpaya@cst.upv.es (J.P.)

* Correspondence: lousomar@upvnet.upv.es

Abstract: Cogeneration with energy cane, a highly productive variety compared to conventional sugarcane, significantly increases ash generation, presenting waste management challenges for the sugar and ethanol industries. This study evaluates the potential of energy cane ash as a sustainable alternative material for partial cement replacement in construction, contributing to circular economy practices. A productivity analysis was conducted for planted areas, and the different parts of sugarcane and energy cane were dried and examined using scanning electron microscopy. These parts were calcined at 450 °C and 600 °C and analyzed using scanning electron microscopy, X-ray fluorescence, particle size distribution, and thermal analysis. The reactivity of the ashes was tested in cement mortars with 5%, 10%, and 20% cement replacement using washed ash. The results revealed that energy cane produces approximately four times more ash per hectare than sugarcane, with leaf ash containing up to 60% silica and stalk ash being rich in potassium. The highest compressive strength was observed in a mortar with 10% cement replacement using washed energy cane ash, achieving 102.43% of the reference value after 28 days of curing, indicating excellent pozzolanic reactivity. These findings highlight the potential of energy cane ash to enhance sustainability in cementitious systems by reducing Portland cement use and promoting waste valorization. Furthermore, the reuse of ash can mitigate waste accumulation and support the development of more sustainable construction materials, contributing to a circular economy and a low-carbon society.

Keywords: sustainable cement composites; sugarcane ash; energy cane ash; waste valorization; phytoliths; chemical composition; pozzolanic materials



Academic Editors: Carlos Miguel Henriques Ferreira, Sara Silva, Catarina Silva S. Oliveira and Alessandra Braga Ribeiro

Received: 16 December 2024

Revised: 9 January 2025

Accepted: 15 January 2025

Published: 20 January 2025

Citation: Lyra, G.P.; Brichi, L.; Roselló, J.; Borrachero, M.V.; Soriano, L.; Payá, J.; Rossignolo, J.A. Energy Cane Ash: Property Assessment for Its Valorization in Sustainable Cementing Systems. *Sustainability* **2025**, *17*, 803. <https://doi.org/10.3390/su17020803>

Copyright: © 2025 by the authors. Licensee MDPI, Basel, Switzerland. This article is an open access article distributed under the terms and conditions of the Creative Commons Attribution (CC BY) license (<https://creativecommons.org/licenses/by/4.0/>).

1. Introduction

Sugarcane is a species of perennial grass belonging to the botanical family *Poaceae* and the genus *Saccharum*. It is a C4 plant, physiologically originating in Asia, cultivated worldwide, and thriving in tropical, subtropical, and temperate climates [1–3]. As a C4 plant, sugarcane exhibits greater photosynthetic efficiency and, consequently, higher carbon fixation, making it one of the plants with the highest dry mass accumulation [4,5].

Currently, commercial sugarcane varieties are hybrids consisting of approximately 80% *Saccharum officinarum*, known for its high sucrose storage, and 20% *Saccharum spontaneum*,

valued for its higher fiber content, which enhances crop resilience and provides essential tolerance to biotic and abiotic stresses [6].

Global sugarcane production reaches an impressive 1.91 billion tons annually [7], underscoring its vital role in the agricultural economy. Brazil, the world's largest producer, leads this industry, with sugarcane serving as a cornerstone of its agribusiness sector. In the 2023/2024 harvest alone, Brazil produced approximately 713.2 million tons of sugarcane [8], reflecting the crop's scale and importance in meeting global demand and driving economic growth.

The production of sugar and ethanol from sugarcane generates significant by-products, namely straw and bagasse. For every ton of sugarcane processed, approximately 25%—equivalent to 250 kg on a dry basis—comprises bagasse and straw [9]. This substantial volume of by-products highlights the potential for resource optimization and valorization within the sugarcane industry, paving the way for more sustainable waste management practices.

Part of these by-products is burned in boilers to generate electricity, reducing the industry's energy costs and enhancing its sustainability [10]. In 2022, sugarcane bagasse accounted for 4.70% of Brazil's electricity generation, a figure expected to grow in the coming years [11]. Unlike other forms of clean energy that merely reduce CO₂ emissions, biomass energy also offers the potential to capture previously emitted CO₂, thanks to carbon fixation via photosynthesis during agricultural production [12].

Approximately 25 kg of ash is generated for every ton of bagasse burned. The chemical composition of sugarcane bagasse ash can vary depending on factors such as the sugarcane variety, soil composition, climate, crop management practices, boiler burning conditions, and the presence of contaminants [13–16].

The ability to produce sugar, ethanol, and electricity has increased the visibility and economic appeal of sugarcane cultivation [17]. Consequently, the sugar and ethanol industry has begun studying another sugarcane species with high biomass production, known as energy cane. This variety was developed for use in producing lignocellulosic ethanol (second-generation ethanol) and as a fuel for biomass boilers to generate electricity. The goal is to meet the industry's energy demands while selling surplus energy to distributors, as energy production is one of the most profitable processes in the sugar and ethanol industries. Given that the ash generated from biomass combustion is expected to increase, studies on its reuse are essential [18–23].

Energy cane is a newly developed variety being extensively studied for cultivation during the sugarcane off-season, on low-fertility soils, for energy generation, and for second-generation ethanol production [6,24,25]. Like sugarcane, energy cane is a hybrid resulting from the backcrossing of *Saccharum officinarum* and *Saccharum spontaneum*, but with a higher contribution from *Saccharum spontaneum*, which increases its fiber content [6]. It is a rhizomatic plant, similar to bamboo, with rhizomes and an extensive root system that allow for greater nutrient absorption from the soil. Unlike sugarcane, which prioritizes sucrose storage, energy cane focuses on fiber production.

These physiological differences result in a cane with a higher sprouting rate that grows taller, thinner, and denser and produces more tillers. Consequently, energy cane achieves significantly higher biomass productivity, averaging about 200 tons per hectare—approximately twice that of sugarcane [6,17,26–29].

When comparing the development of sugarcane and energy cane, sugarcane begins by sprouting roots, whereas energy cane develops buds and, shortly after, surpasses sugarcane in size and root development [4,6,27]. The primary difference lies in the stalk diameter; sugarcane typically has a larger diameter. The stalk diameter is directly related to fiber content: the smaller the diameter, the higher the fiber content, as fibers are concentrated in

greater amounts in the bark. Thus, a smaller diameter results in a higher surface area-to-volume ratio [27,30].

The greater fiber-to-energy gain in energy cane results in a decrease in sucrose content because, after photosynthesis, carbon is distributed among sucrose storage, respiration, and cell wall biosynthesis [31]. Although sugarcane contains a higher concentration of sucrose, the per-hectare sucrose production is estimated to be similar to that of energy cane due to the latter's higher productivity [32].

Several studies have focused on the cultivation, productivity, energy generation, and lignocellulosic ethanol production from energy cane [11,18,22,27,29,33,34]. However, research on the ash composition, waste from energy cogeneration, and its potential applications remains limited.

Incorporating agro-industrial waste into cement composites offers a viable solution for recycling and reuse, promoting a circular economy. The cement matrix can accommodate waste materials, reducing landfill disposal and conserving natural resources used in fabricating these composite materials [35].

Sugarcane ash contains silicon, a key component of interest for cement composites. Amorphous-phase silica (SiO_2) in the ash exhibits pozzolanic properties, enabling it to react with portlandite released during Portland cement hydration and form insoluble cementitious compounds [36].

The presence of SiO_2 in plants arises from silicon absorbed from the soil by the roots as monosilicic acid (H_4SiO_4). Upon water loss through transpiration, silicon is deposited as silica gel on the outer walls of epidermal cells. Additionally, sugarcane is often contaminated with sand during harvesting, which introduces crystalline silica in the form of quartz [37–39]. Monocotyledonous plants, particularly those in the *Poaceae* family (e.g., sugarcane, energy cane, rice, and bamboo), are known to accumulate silicon [40].

Plants also contain specialized cells called phytoliths or silico-phytoliths, whose primary component is silica. The morphology of these structures varies by plant type, with common shapes including saddle, dumbbell, and cross forms [41,42].

Numerous studies indicate that sugarcane ash has a chemical composition suitable for use as a pozzolanic mineral additive in Portland cement composites [43]. For instance, Kolawole et al. (2021) [44] conducted a comprehensive literature review of over 100 studies on sugarcane ash in cementitious materials. These studies confirm that sugarcane ash is a pozzolanic material capable of reacting with calcium hydroxide during cement hydration.

While extensive research exists on sugarcane ash, the properties and potential applications of energy cane ash have not yet been thoroughly investigated.

Thus, recognizing the need to characterize energy cane ash and explore its efficient use, this study aimed to analyze the ash produced from the combustion of various parts of energy cane, comparing it with sugarcane ash. The objective was to evaluate the presence of silica and other components, thereby providing data to support and stimulate future applications in cement composites.

2. Materials and Methods

The energy cane samples (VIGNIS 5) were collected in Santo Antônio de Posse (São Paulo, Brazil), and the sugarcane samples (RB 867515) were collected in Pirassununga (São Paulo, Brazil). Both collections were conducted in the field immediately before harvest, ensuring all parts of the cane were preserved.

Deformed soil samples were collected from the 0–20 cm and 20–40 cm layers, homogenized into composite samples, air-dried, sieved using a 2 mm mesh, and sent for chemical analysis following the methodology described by Raij et al. (2001) [45]. Based on the pedological map of São Paulo State and the properties' locations, the soil where the

energy cane was collected is classified as a typical dystrophic red-yellow latosol, while the soil for the sugarcane is characterized as dystroferric red latosol [46].

Table 1 presents the chemical characteristics of the soils analyzed for energy cane and sugarcane.

Table 1. Chemical characterization of the soil obtained in the 0–20 and 20–40 cm layers from energy cane and sugarcane collection sites.

Elements	Units	Energy Cane	Sugarcane	Energy Cane	Sugarcane
		0–20 cm		20–40 cm	
pH	CaCl ₂	5.6	5.4	5.3	5.3
P resin	mg·m ^{−3}	36	16	7	13
S		12	10	34	11
K resin		4	2.9	2.8	2.7
Ca	m molc·dm ^{−3}	38	26	25	23
Mg		19	6	9	4
Al		0	0	0	0
H + Al		26	21	24	20
MO ^a	g·kg ^{−1}	23	16	18	16
COT ^b		13.2	9.6	10.1	9.1
B	mg·dm ^{−3}	0.84	0.32	0.59	0.3
Cu		8.4	0.9	1.8	1.2
Fe		38	32	23	35
Mn		16.1	1.7	2.1	3.1
Zn		9.3	3.9	0.3	3.5
SB ^c	m molc·dm ^{−3}	61	35	37	30
CTC ^d		87	56	60	50
V ^e	%	70	62	61	59

^a Organic matter, ^b total carbon, ^c base sum, ^d cation exchange capacity, ^e saturation.

For both energy cane and sugarcane, productivity evaluations were conducted by weighing the fresh mass and its parts (stalk and leaf) per planted area.

After collection, the canes were thoroughly washed to remove residual soil contamination. Following washing, they were dried in an oven at 100 ± 5 °C until reaching a constant mass and subsequently separated into stalks and leaves.

For the morphological analysis of the different parts of energy cane and sugarcane, sections of the stalk, leaves, and veins of both varieties were prepared for observation under a scanning electron microscope (SEM), ZEISS ULTRA 55 (Zeiss, Oberkochen, Germany).

The different cane sections were calcined at 450 °C for 1 h at a heating rate of 10 °C/min in a muffle furnace (Carbolite RHF model 1500, Hope Valley, UK) for morphological and compositional analysis. This temperature was chosen to preserve the skeletal cellular structure of energy cane and sugarcane, as higher temperatures would lead to complete disintegration. The ash was subsequently analyzed using the ZEISS ULTRA 55 SEM, and energy-dispersive X-ray spectroscopy (EDS) was employed to identify the primary elements in the ash. The EDS analysis was conducted using the SDD X-Max 20 mm² detector from Oxford Instruments (Abingdon, UK) and processed with AZtec 3.3 SP1 software from Oxford Instruments (Abingdon, UK).

For further ash studies, the stalks and leaves of energy cane and sugarcane were calcined at 600 °C for 2 h in a resistive oven (model 10013, 7000 W power, Jung, Blumenau, Santa Catarina, Brazil). The ash was immediately removed after firing and cooled at room temperature (25 ± 3 °C). This temperature was selected as it allows for complete removal of organic matter without altering the mineralogy of the compounds [15,37].

Chemical analysis of the raw materials was performed using an X-ray fluorescence (XRF) spectrometer (MiniPal4 model, Malvern PANalytical, Malvern, UK). Loss on ignition (LOI) was determined at 1100 °C for 1 h, following the ASTM C114:18 standard [47].

The particle size distribution of the ash was measured using a Horiba Laser Particle Size Analyzer (LA-950V2 model, Horiba Ltd., Kyoto, Japan), with isopropyl alcohol as the dispersion medium to prevent reactivity. The specific mass of the ash was determined using a helium gas multipycnometer (model 1000, Quantachrome Instruments, Boynton Beach, FL, USA).

The mineralogical composition of the raw materials was analyzed using X-ray diffraction (XRD) with a Rigaku miniFlex 600 diffractometer (Rigaku, Akishima, Tokyo, Japan) equipped with a graphite monochromator in the secondary beam. The XRD system operated at 40 V/15 mA with a scanning range of $2^\circ \leq 2\theta \leq 90^\circ$ and a scan speed of $1^\circ/\text{min}$.

Thermal analyses of the ash were conducted using a NETZSCH STA449 F3 Jupiter system (NETZSCH, Selb, Germany), which combines differential thermal analysis (DTA), thermogravimetric analysis (TGA), and differential scanning calorimetry (DSC). The tests were performed at a heating rate of 10 °C/min in a nitrogen atmosphere (flow rate: 20 mL/min), with initial and final temperatures of 25 °C and 1100 °C, respectively.

To evaluate the reactivity of the ash, a compressive strength test was conducted on mortars with varying levels of cement replacement by ash. For this analysis, a mixture of ash from stalks and leaves was used.

To extract soluble products, particularly potassium, chlorine, and sulfur, the ashes burned at 600 °C were mixed for 5 min in batches of 5 g with 500 mL of deionized water at 60 °C using a magnetic stirrer (C-MAG HS 10–220 V, IKA, Staufen, Germany) and then filtered (qualitative filter paper, 160 mm diameter, 205 µm thickness, 80 g/m² weight). A second washing was performed, in which the ashes were stirred with 200 mL of deionized water at 60 °C for 3 h, filtered, and dried in an oven at 60 °C for 24 h [48].

The chemical composition of the washed raw materials was analyzed using an X-ray fluorescence spectrometer (MiniPal4 model, Malvern PANalytical, Malvern, UK) to verify washing efficiency. Loss on ignition (LOI) was determined at 1100 °C for 1 h, following ASTM C114:18 [47].

Mortars with a mix ratio of 1:2.5:0.5 (cement/sand/water) by mass were evaluated with different levels of replacement using washed energy cane and sugarcane ash (0%, 5%, 10%, and 20%), along with a 10% replacement using silica fume as a comparison to a commercial pozzolan. These proportions were chosen because they represent the mortar dosage typical of traditional concrete, with a cement consumption of approximately 300 kg/m³, a sand content of 750 kg/m³, and a water/binder ratio of 0.5 [49].

The mortar specimens were molded into cylindrical shapes measuring 5 cm × 10 cm (diameter × height) and cured under wet conditions (RH = $95 \pm 2\%$) at a temperature of 25 ± 2 °C until the specified testing ages (7 and 28 days). Table 2 presents all the mortar compositions and the naming conventions used for the presentation of results.

For the compressive strength test, five specimens of each mixture were tested at 7 and 28 days for each dosage studied, in accordance with ABNT NBR 5739:2007 [50]. The test was conducted using an EMIC universal testing machine, model DL-30000 (EMIC, São José dos Pinhais, Paraná, Brazil), equipped with a 50 kN load cell.

Table 2. Mortars and acronyms used to present the results.

Mortars	Acronyms
Mortar Reference	Reference
Mortar with 10% Silica fume	Silica fume
Mortar with 5% sugarcane ash	SCA-W-5
Mortar with 10% sugarcane ash	SCA-W-10
Mortar with 20% sugarcane ash	SCA-W-20
Mortar with 5% energy cane ash	V5-W-5
Mortar with 10% energy cane ash	V5-W-10
Mortar with 20% energy cane ash	V5-W-20

3. Results and Discussion

3.1. Soil Chemical Analysis

According to the chemical characterization of the studied soil (Table 1) and based on the interpretation proposed by Raij et al. (2001) [45], phosphorus levels are moderate in the 0–20 cm layer, while calcium and magnesium levels are high for both energy cane and sugarcane. Potassium levels are considered high for energy cane and moderate for sugarcane in this same layer.

The V% represents the percentage of soil saturation by exchangeable bases. A value above 50% is ideal for ensuring nutrient availability from the soil to the plant, indicating fertile soil. Base saturation is adequate, with sugarcane soil showing a V% of 62% at a 0–20 cm depth and 59% at a 20–40 cm depth. Similarly, the soil of energy cane exhibits a V% of 70% at a 0–20 cm depth and 61% at a 20–40 cm depth; both percentages are considered satisfactory.

Regarding micronutrients, their levels range from high to moderate for energy cane and sugarcane, respectively, in the 0–20 cm layer. Interestingly, there is an accumulation of sulfur in the 20–40 cm layer in areas cultivated with energy cane.

3.2. Productivity Evaluations

The materials analyzed demonstrated a sugarcane productivity of 90 t/ha and an energy cane productivity of 180 t/ha. Sugarcane composition was 70% water, 20.61% stalk, and 9.39% straw, while energy cane comprised 50% water, 34.83% stalk, and 15.17% straw. After burning, the ash yields were as follows: sugarcane produced 1.36% stalk ash and 3.73% straw ash, whereas energy cane produced 2.00% stalk ash and 5.27% straw ash.

When scaled to one hectare, sugarcane generated 252 kg of stalk ash and 315 kg of straw ash, totaling 567 kg of ash per hectare. In contrast, energy cane produced 1260 kg of stalk ash and 1440 kg of straw ash, amounting to 2700 kg of ash per hectare. These results indicate that energy cane generates approximately four times more ash per hectare than conventional sugarcane, emphasizing the importance of studying its properties to ensure proper and sustainable utilization of this by-product.

3.3. Morphological Analysis of the Different Parts of the Energy Cane and Sugarcane

Figure 1 shows the micrographs of sugarcane and energy cane stalks dried at 105 °C. As expected, none of the micrographs display phytoliths, trichomes, or other identifiable elements, as the stem primarily consists of fibers and the central region where sucrose is concentrated.

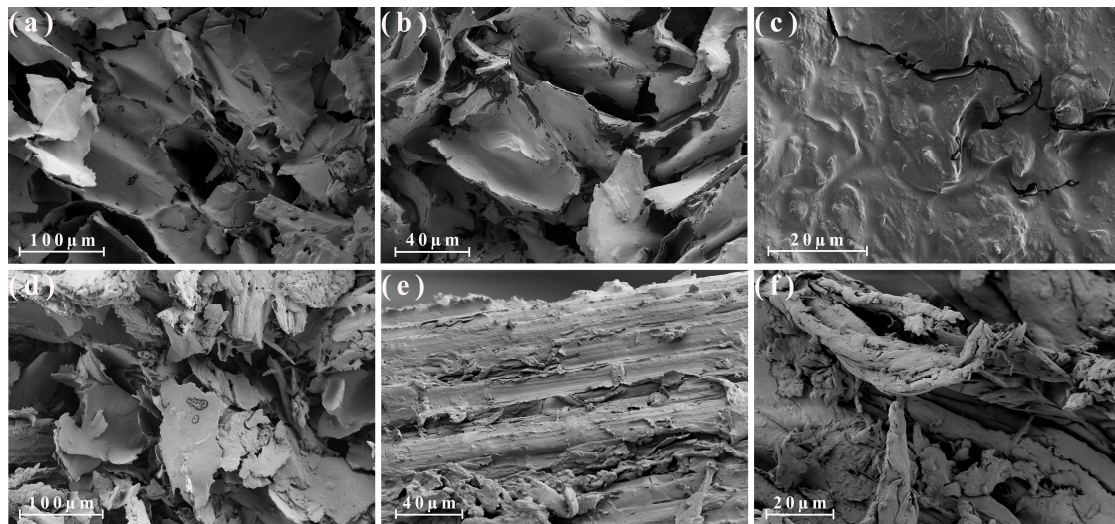


Figure 1. SEM micrographs of 105 °C dried stalk. Sugarcane (a–c). Energy cane (d–f).

Figure 2 presents micrographs of the abaxial side of leaves dried at 105 °C, showing sugarcane (a, b, c) and energy cane (d, e, f). Figure 2a provides an overview of the sugarcane leaf's abaxial epidermis, revealing rows of stomata and trichomes of short and prickle thickness arranged in parallel. Figure 2b highlights stomata in detail, along with a dumbbell-shaped phytolith aligned with the leaf's longitudinal axis, while Figure 2c provides a close-up of a dumbbell-shaped phytolith.

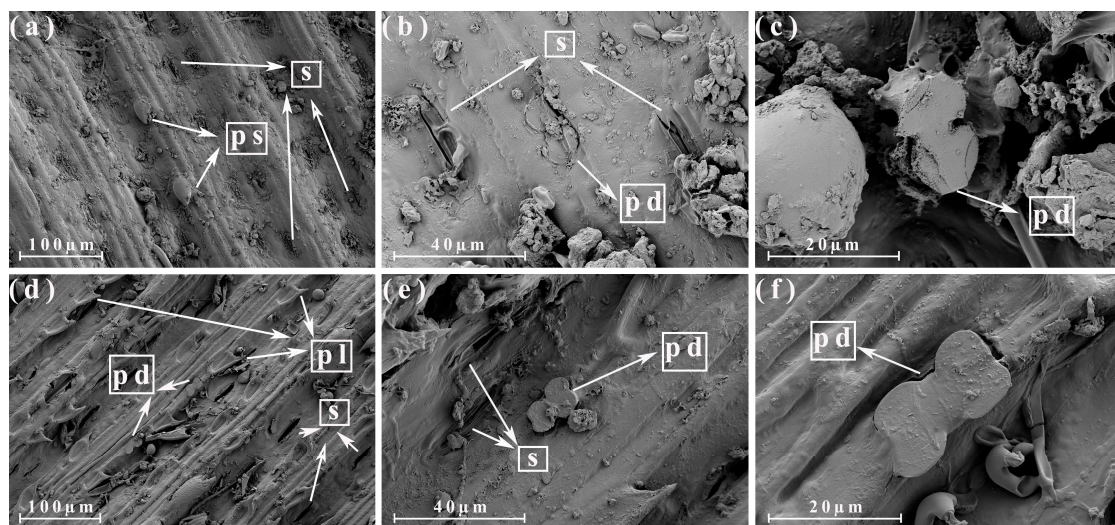


Figure 2. SEM micrographs of 105 °C dried abaxial leaf. Sugarcane (a–c). Energy cane (d–f). (pd) Dumbbell phytolith, (pl) prickly large trichomes, (ps) prickly short-thick trichomes, (s) stoma.

Figure 2d illustrates stomata parallel to large prickly trichomes and dumbbell-shaped phytoliths in the longitudinal direction of the energy cane leaf. Figure 2e shows stomata, a dumbbell-shaped phytolith, and a wide trichome, and Figure 2f provides an enlarged view of a dumbbell-shaped phytolith. From these images, no discernible differences between the abaxial surfaces of sugarcane and energy cane leaves can be observed.

Figure 3 presents micrographs of the adaxial side of leaves dried at 105 °C, showing sugarcane (a, b, c) and energy cane (d, e, f). The images show no significant differences compared to those from the abaxial region.

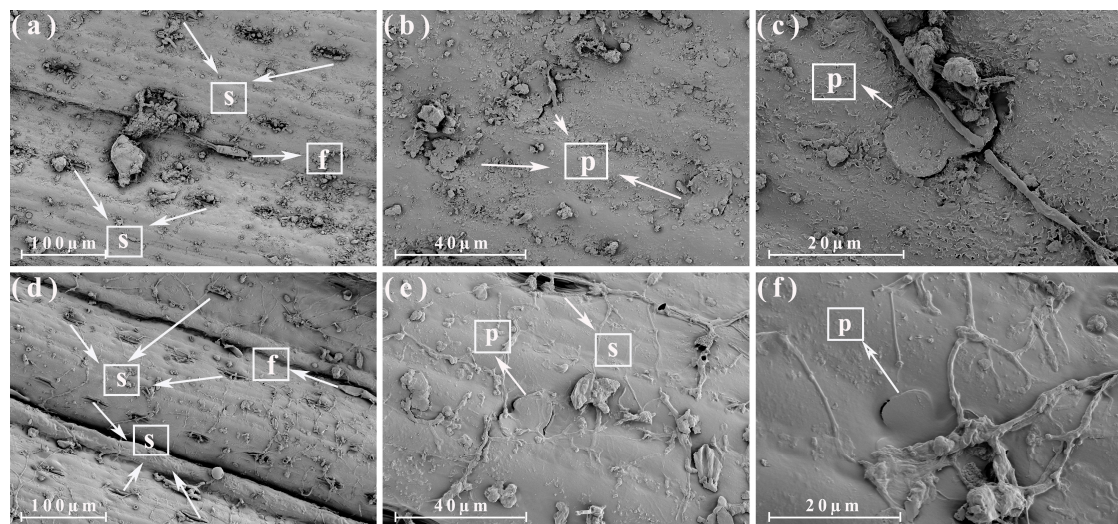


Figure 3. SEM micrographs of 105 °C dried adaxial leaf. Sugarcane (a–c). Energy cane (d–f). (f) Filiform hairs, (p) phytolith, (s) stoma.

Figure 3a provides an overview where stomata and a large trichome (filiform hair) can be observed. In Figure 3b, some phytoliths are identified, while Figure 3c shows an enlarged view of a phytolith. Similarly, the energy cane overview (Figure 3d) also reveals stomata and a large trichome. Figure 3e shows a stoma and a phytolith, and Figure 3f provides a close-up of a phytolith.

In the images of the abaxial central nerve of the leaves, no phytoliths, trichomes, or other notable features were observed. Figure 4 shows micrographs of the adaxial central nerve of leaves dried at 105 °C, depicting sugarcane (a, b, c) and energy cane (d, e, f).

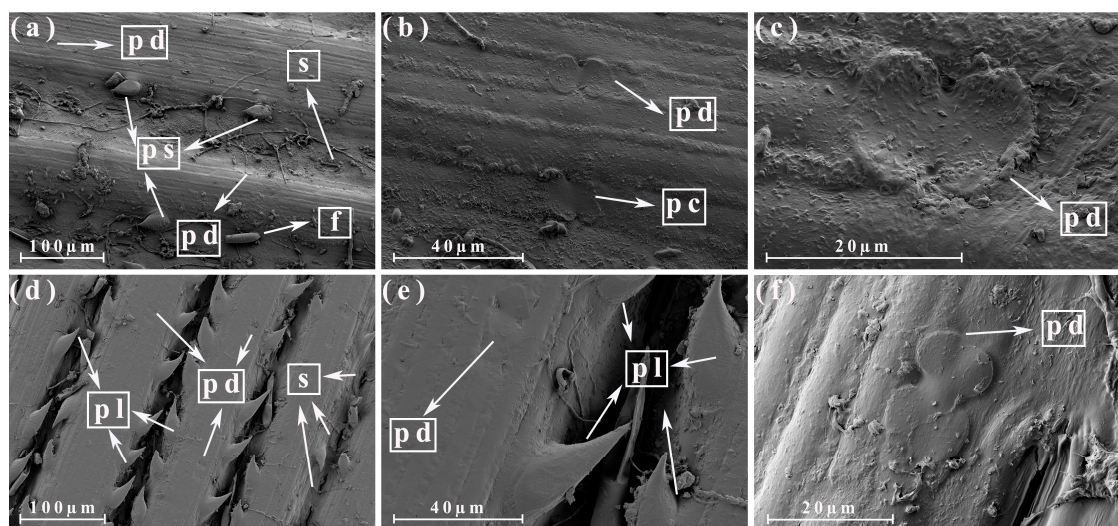


Figure 4. SEM micrographs of 105 °C dried adaxial of the leaf's central nerve. Sugarcane (a–c), energy cane (d–f). (f) filiform hairs, (ps) prickly short-thick trichomes, (pl) prickly large trichomes, (pd) dumbbell phytolith, (pc) cross phytolith, (s) stoma.

Figure 4a provides an overview of the sugarcane adaxial nerve, showing stomata, short and prickly trichomes, dumbbell-shaped phytoliths, and a wide trichome, all aligned in the longitudinal direction. Figure 4b highlights the presence of both dumbbell-shaped and cross-shaped phytoliths, while Figure 4c offers a close-up of a dumbbell-shaped phytolith.

In contrast, Figure 4d presents an overview of the energy cane adaxial nerve, revealing rows of large prickly trichomes arranged parallel to the stomata in greater numbers than

observed in sugarcane, alongside dumbbell-shaped phytoliths. Figure 4e shows details of enlarged prickly trichomes and a dumbbell-shaped phytolith, while Figure 4f provides a close-up view of a dumbbell-shaped phytolith.

3.4. Morphological Analysis of the Different Parts of the Energy Cane Ash and Sugarcane Ash

Figure 5 shows micrographs of stalks calcined at 450 °C for sugarcane (a, b, c) and energy cane (d, e, f). Similar to the images of the dried sugarcane stalks, no identifiable elements are observed. However, micrographs Figure 5d,f of the energy cane ash reveal particles referred to as α , which are rich in potassium and chlorine. An EDS analysis of the α particle in image 5f detected K₂O (58.11%) and Cl (41.89%).

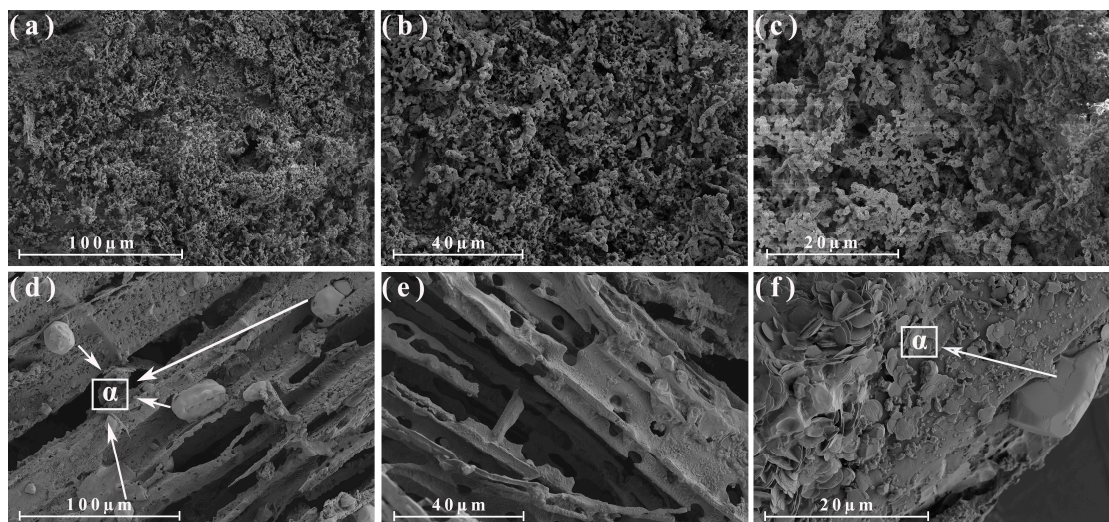


Figure 5. SEM micrographs of the stalk calcined at 450 °C. Sugarcane (a–c). Energy cane (d–f). (α) Potassium-rich particles.

Figure 6 shows micrographs of leaves calcined at 450 °C for sugarcane (a, b, c) and energy cane (d, e, f). No distinction could be made between the adaxial and abaxial sides because the leaves disintegrated during calcination, making it impossible to identify the surfaces.

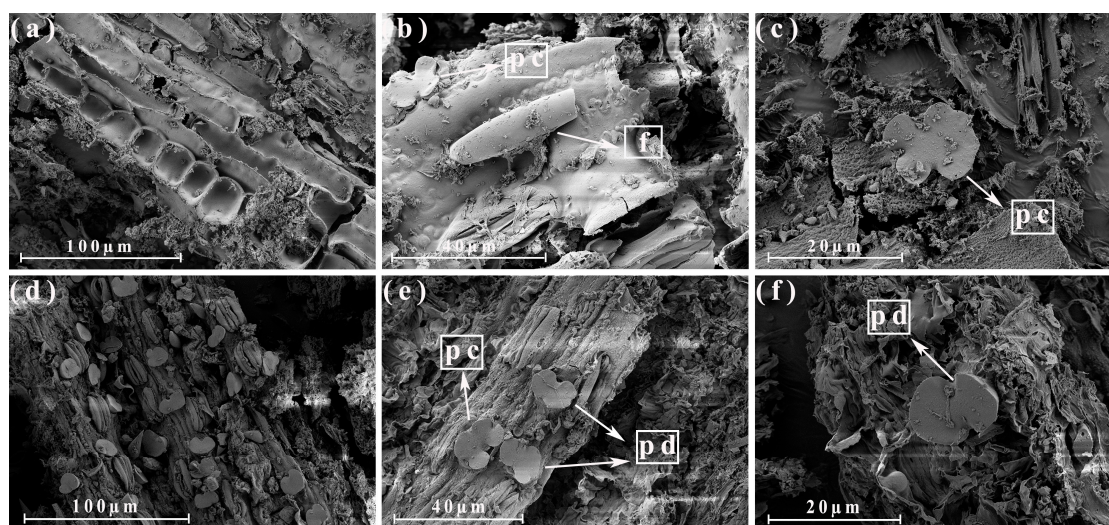


Figure 6. SEM micrographs of the leaf calcined at 450 °C. Sugarcane (a–c). Energy cane (d–f). (f) Filiform hair, (pd) dumbbell phytolith, (pc) cross phytolith.

Figure 6a provides an overview of the sugarcane leaf ash, showing the interior of the epidermal cells, where large cells with scalloped walls and short cells with smooth walls can be observed. Figure 6b highlights the presence of a cross-shaped phytolith and a broad trichome. Figure 6c presents a magnified view of a cross-shaped phytolith analyzed by EDS, which identified SiO_2 (85.49%) and K_2O (14.51%), as well as amorphous material surrounding it.

Figure 6d provides an overview of the energy cane leaf ash, showing several dumbbell- and cross-shaped phytoliths along with stomata. Figure 6e highlights two dumbbell-shaped phytoliths and a cross-shaped phytolith. Figure 6f presents a magnified view of a dumbbell-shaped phytolith, which EDS analysis identified as containing SiO_2 (97.26%), K_2O (2.25%), MgO (0.49%), and amorphous material.

From these images, it is evident that the energy cane leaf ash contains a greater abundance of phytoliths compared to sugarcane leaf ash. This observation aligns with the chemical composition data presented in Table 3, which shows that energy cane leaf ash has a higher silica content.

Table 3. Chemical compositions of ashes determined by the XRF analysis (wt. %).

Oxides (%)	Stalk		Leaf		Mixed Ash (Stalk + Leaf)	
	Sugarcane	Energy Cane	Sugarcane	Energy Cane	Sugarcane	Energy Cane
MgO	9.9	3.86	12.65	8.48	11.34	6.43
SiO_2	6.34	4.46	28.47	45.73	18.82	27.11
P_2O_5	6.09	5.51	2.97	2.87	4.42	4.18
SO_3	10.17	4.21	13.08	5.56	11.93	5.01
K_2O	62.87	47.48	19.07	11.37	38.29	27.75
CaO	0	6.41	20.86	21.42	11.6	14.64
TiO_2	0	0	0	0.21	0	0.11
MnO	0	0.06	0.31	0.25	0.17	0.17
Fe_2O_3	0.06	0.12	0.42	1.13	0.27	0.67
BaO	0	0	0.18	0.1	0.1	0.06
Cl	4.3	27.5	1.82	2.66	2.85	13.58
LOI	0.27	0.39	0.17	0.22	0.21	0.30

Figure 7 shows micrographs of the abaxial central nerve of leaves calcined at 450 °C for sugarcane (a, b, c) and energy cane (d, e, f). In the sugarcane ash images, phytoliths are not observed. However, stomata (Figure 7a), enlarged silica-rich cell walls (Figure 7b), and broad trichomes (Figure 7c) can be seen.

In contrast, phytoliths are visible in the ash from the energy cane nerve. The overview (Figure 7d) reveals numerous crossed stomata, dumbbell-shaped phytoliths, and other phytoliths aligned primarily in the longitudinal direction of the leaf axis. This alignment is characteristic of sugarcane and likely energy cane, as it is a related variety with shared ancestors. However, the calcination process can influence the orientation of phytoliths [51]. Figure 7e highlights stomata, dumbbell-shaped phytoliths, and cross-shaped phytoliths. Figure 7f shows two enlarged dumbbell-shaped phytoliths.

An EDS analysis of one of these phytoliths revealed the following composition: SiO_2 (97.16%), K_2O (2.07%), and CaO (0.77%). Similar to the leaf ash, the energy cane abaxial central nerve ash contained a higher abundance of phytoliths, as observed in the overview.

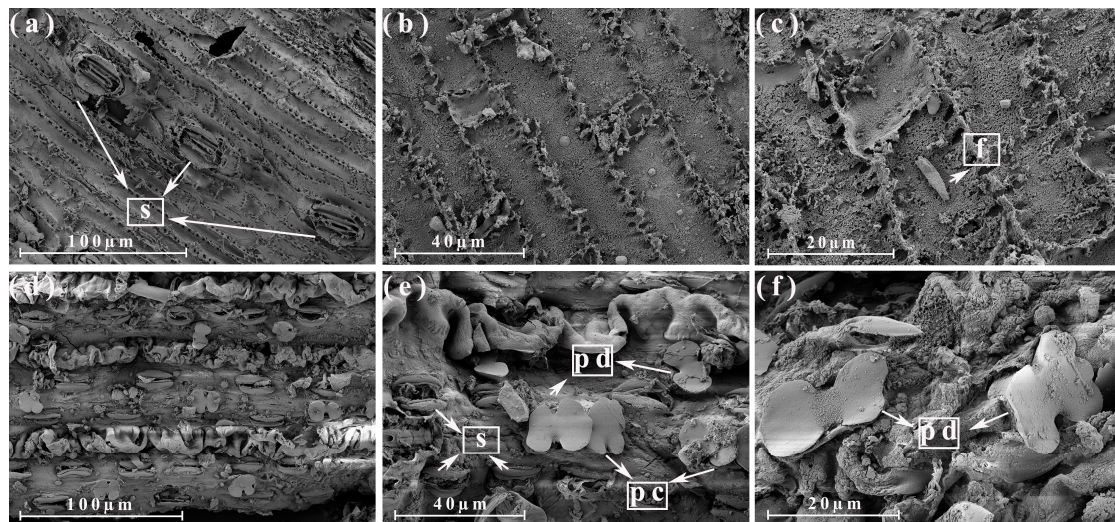


Figure 7. SEM micrographs of the abaxial central nerve of the leaf calcined at 450 °C. Sugarcane (a–c). Energy cane (d–f). (f) Filiform hair, (pd) dumbbell phytolith, (pc) cross phytolith, (s) stoma.

Figure 8 shows micrographs of the adaxial central nerve of leaves calcined at 450 °C for sugarcane (a, b, c) and energy cane (d, e, f).

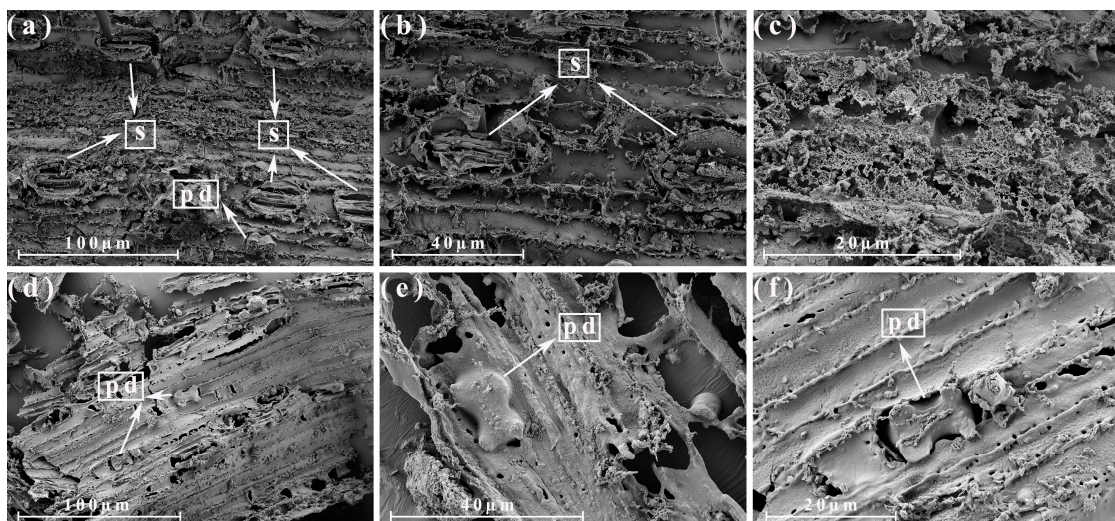


Figure 8. SEM micrographs of the adaxial of the leaf's central nerve calcined at 450 °C. Sugarcane (a–c). Energy cane (d–f). (pd) Dumbbell phytolith, (s) stoma.

In contrast to the abaxial region of sugarcane (Figure 7a–c), Figure 8a reveals the presence of a phytolith in the adaxial region.

Figure 8d–f for energy cane show a greater abundance of dumbbell-shaped phytoliths aligned along the longitudinal axis of the leaf.

3.5. Chemical Determination of the Ash

Table 3 presents the composition of oxides found in the ash from selected parts of the plants. The nutrients absorbed by plants are influenced by the genetic characteristics of the varieties and the availability of these nutrients in the soil. These nutrients remain in the ash after the burning of sugarcane and energy cane [52].

Potassium is the nutrient most absorbed by sugarcane during its development. It exhibits high mobility within the plant and is absorbed by various parts, with the stalk accumulating significantly more than the leaves [53]. Both sugarcane and energy cane

absorb potassium in substantial amounts without negatively affecting productivity [54,55], which explains the high potassium content observed in the ash. Potassium functions as an enzyme activator in photosynthesis, protein synthesis, sucrose translocation, and other physiological processes [56].

The high potassium content in ash can, however, contribute to a degradation process when incorporated into cement matrices due to the alkali-aggregate reaction [57]. Potassium oxide reacts with certain aggregates, leading to concrete disintegration [58]. To mitigate this, potassium can be extracted from the ash and repurposed as a fertilizer in agriculture. The resulting ash, after potassium removal, would have a higher silica content, making it suitable for use in cementitious composites.

Chlorine is absorbed by roots and leaves in significant amounts in the form of Cl^- when available in the soil. It has high mobility within the plant and plays a role in photosynthesis, water metabolism, and transpiration. Chlorine is particularly important for C4 plants like sugarcane and energy cane [59]. However, a high chloride ion concentration in reinforced concrete can cause reinforcement corrosion, one of the leading causes of structural degradation. This corrosion occurs through an electrochemical process involving anodic and cathodic reactions, causing the reinforcement to expand and crack the concrete [60,61]. Like potassium, chlorine can also be extracted from the ash through a washing process due to its water solubility. However, chlorine evaporates quickly, making it unsuitable for long-term storage in chlorinated water.

In the later stages of development, sugarcane absorbs magnesium, with approximately 2.7% of chlorophyll molecules consisting of magnesium [62].

Calcium is required in appropriate amounts in crops. It plays a crucial role in cell wall structure, membrane integrity, and other physiological functions, as well as in correcting soil pH [55]. For sugarcane cultivation, the soil typically undergoes a liming process, where lime is applied to increase calcium availability, which in turn influences the calcium content in the plant.

Sugarcane is a silicon-accumulating crop, absorbing silicon from the soil in the form of monosilicic acid (H_4SiO_4) [63]. Silicon is considered beneficial for certain crops, including sugarcane [55]. A significant portion of the silicon absorbed by the plant is concentrated in the leaves, specifically in the epidermal tissues just beneath the cuticle and, more precisely, in the outermost cell walls [64,65]. Silicon contributes to plant structure and enhances photosynthesis by keeping the leaves more erect, thereby preventing self-shading. This results in increased plant height due to the elongation of leaf blades [65–67].

As shown in the analysis, the leaves contain a significantly higher amount of silicon compared to the stalks in both types of cane studied: for sugarcane, 6.34% in the stalk versus 28.47% in the leaf, and for energy cane, 4.46% in the stalk versus 45.73% in the leaf.

Due to the high silicon content in sugarcane ash, numerous studies have explored its potential as a pozzolan in cement composites [8,48,68]. Lyra et al. (2021) [48] propose washing sugarcane ash to remove excess potassium, which is detrimental to cement matrices. The potassium-rich water from this process could be repurposed as a fertilizer, while the washed ash could be used as a pozzolan.

The minimum required content for the sum of SiO_2 , Al_2O_3 , and Fe_2O_3 oxides in pozzolans to be combined with cement is 50% [69]. Before washing, the general ash (a mixture of stalk and leaf ash) from both sugarcane and energy cane did not meet this requirement, with totals of only 19.09% and 27.78%, respectively. Additionally, the maximum allowable alkali content of 1.5% and sulfuric oxide content of 5% were also exceeded. Mixed sugarcane ash contained 38.29% alkali and 11.93% sulfuric oxide, while mixed energy cane ash contained 27.79% alkali and 5.01% sulfuric oxide.

To address these issues, a washing and filtering process was applied to extract alkalis and sulfuric oxide, as well as part of the chlorine. This process significantly reduced potassium and sulfuric oxide levels and increased the concentration of other oxides, particularly silicon, as expected (Table 4). After washing, the mixed sugarcane ash showed a sum of SiO_2 , Al_2O_3 , and Fe_2O_3 of 53.64% and sulfuric oxide content of 0.5%. Similarly, mixed energy cane ash reached 60.18% for the sum of SiO_2 , Al_2O_3 , and Fe_2O_3 , with sulfuric oxide content reduced to 0.66%.

Table 4. Chemical compositions of washed ashes determined by the XRF analysis (wt. %).

Oxides (%)	Washed					
	Stalk		Leaf		Mixed Ash (Stalk + Leaf)	
	Sugarcane	Energy Cane	Sugarcane	Energy Cane	Sugarcane	Energy Cane
MgO	26.96	20.15	9.93	5.12	16.02	10.75
SiO_2	34.92	40.67	60.59	65.16	51.42	58.49
P_2O_5	9.19	15.97	2.74	2.5	5.04	6.36
SO_3	0	0	0.77	0.92	0.5	0.66
K_2O	7.36	5.39	5.16	6.35	5.95	4.5
CaO	17.76	13.56	16.77	16.58	17.12	15.39
TiO_2	0.27	0.75	0.42	0.43	0.37	1.2
MnO	0.62	0.23	0.5	0.22	0.54	0.25
Fe_2O_3	2.23	0.53	2.36	1.78	2.22	1.69
BaO	0	0	0	0	0.09	0
ZnO	0	0	0.27	0.13	0.32	1.44
Cl	0.17	2.29	0.41	0.46	0.1	0.04
LOI	0.25	0.33	0.35	0.47	0.31	0.43

In terms of alkali content, both ashes still exceeded the maximum permissible level of 1.5%. However, after washing, the alkali content dropped significantly, reaching 5.95% for mixed sugarcane ash and 4.5% for mixed energy cane ash. Regarding the loss on ignition (LOI), all ashes fell within the recommended limit of below 6%, as specified by the standard [69].

Similar to sugarcane ash, energy cane leaf ash contains substantial levels of silica, suggesting its potential use as a pozzolan.

3.6. Particle Size Distribution of the Ash

Table 5 presents the equivalent particle size of sugarcane stalk ash (SCA-S), sugarcane leaf ash (SCA-L), energy cane stalk ash (V5-S), and energy cane leaf ash (V5-L). The data show that the average particle diameters of the ash derived from the stalks are smaller for both types of cane compared to those from the leaves. This difference may be attributed to the composition of the ash, as silicon oxide, which constitutes the majority of the stalk ash, tends to form smaller particles compared to potassium oxide, which is more abundant in the leaves.

Table 5. Equivalent particle diameters.

Ashes	*D ₁₀ (μm)	*D ₅₀ (μm)	*D ₉₀ (μm)	*D _{mea} (μm)
SCA-S	0.08	11.55	179.65	51.38
SCA-L	9.95	49.64	170.97	67.04
V5-S	0.12	19.41	133.91	40.15
V5-L	9.37	47.34	164.34	65.03

*D₁₀, D₅₀, and D₉₀ are the maximum particle sizes that compose 10%, 50%, and 90% of sample volume, respectively. D_{mea} = mean particle size.

3.7. Specific Mass of the Ash

The specific mass is associated with the internal porosity of the particles [62], which can influence the density of materials produced using these ashes. Sugarcane exhibited a specific mass of 2.54 ± 0.01 for stalk ash and 2.46 ± 0.01 for leaf ash, while energy cane showed a specific mass of 2.40 ± 0.01 for stalk ash and 2.46 ± 0.01 for leaf ash. The specific mass values for both types of ash are very similar.

3.8. Mineralogical Composition Analysis of the Ash

Figure 9 and Table 6 present the X-ray diffractograms and mineralogical components of SCA-S, SCA-L, V5-S, and V5-L. The sugarcane stalk ash (SCA-S) exhibited major peaks corresponding to sylvine, arcanite, and potassium oxide, indicating a significant presence of potassium. This result aligns with the chemical composition shown in Table 3, which reports approximately 63% potassium oxide in the sugarcane stalk ash.

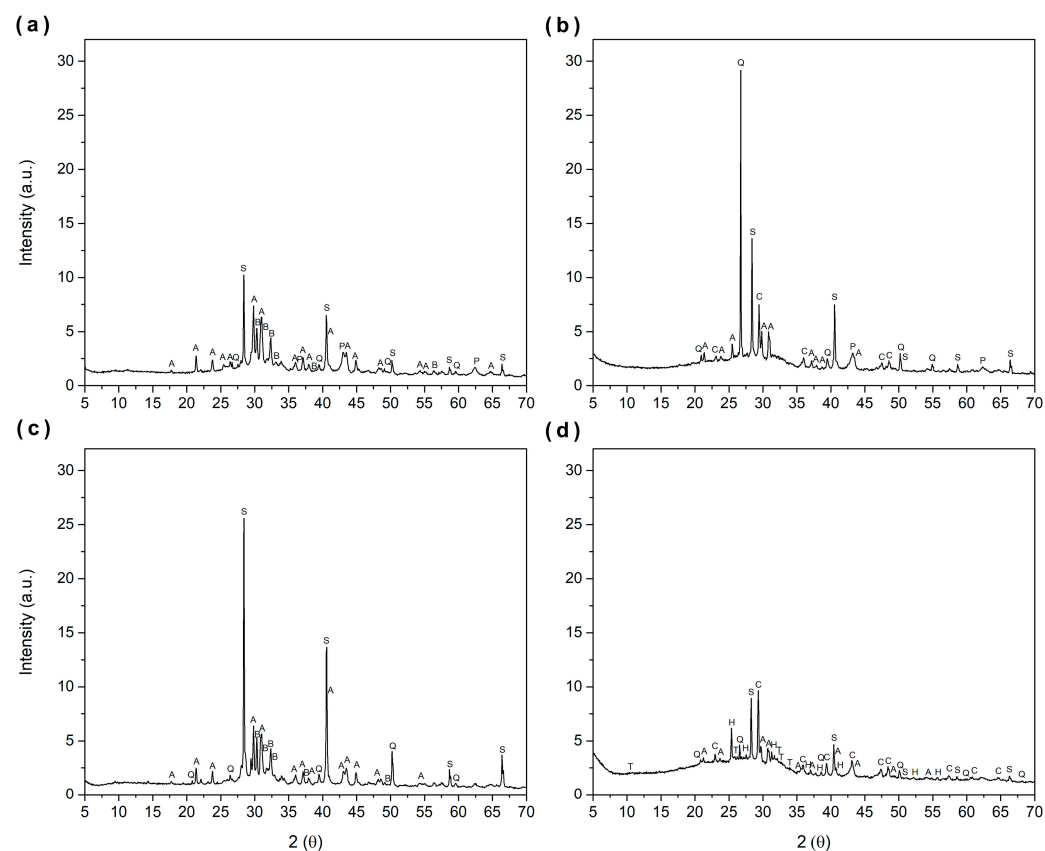
**Figure 9.** X-ray diffractograms of (a) SCA-S, (b) SCA-L, (c) V5-S, and (d) V5-L.

Table 6. Mineralogical composition of SCA-S, SCA-L, V5-S, and V5-L crystalline solids.

Ashes	Abbreviation	Mineralogical Name	Chemical Formula	PDFcard
SCA-S	S	Sylvine	KCl	411476
	A	Arcanite	K ₂ SO ₄	50613
	Q	Quartz	SiO ₂	331161
	B	Potassium oxide	K ₂ O	270431
	P	Periclase	MgO	40289
SCA-L	S	Sylvine	KCl	411476
	A	Arcanite	K ₂ SO ₄	50613
	Q	Quartz	SiO ₂	331161
	P	Periclase	MgO	40289
	C	Calcite	CaCO ₃	50586
V5-S	S	Sylvine	KCl	411476
	A	Arcanite	K ₂ SO ₄	50613
	Q	Quartz	SiO ₂	331161
	B	Potassium oxide	K ₂ O	270431
V5-L	S	Sylvine	KCl	411476
	A	Arcanite	K ₂ SO ₄	50613
	Q	Quartz	SiO ₂	331161
	C	Calcite	CaCO ₃	50586
	H	Anhydrite	CaSO ₄	371496
	T	Hydroxyapatite	Ca ₅ (PO ₄) ₃ (OH)	90432

In contrast, the sugarcane leaf ash (SCA-L) displayed major peaks of quartz, calcite, sylvine, and arcanite. These minerals correspond to the primary oxides identified by XRF analysis, namely silicon, calcium, and potassium oxides. The higher silicon content in the leaves is consistent with its structural role, supporting photosynthesis. Interestingly, quartz is identified as a mineral component despite silica in plant cells typically being amorphous. The quartz presence is likely due to soil particles adhering to plant tissues, as the ash formation temperature is relatively low.

Similarly to SCA-S, the energy cane stalk ash (V5-S) showed major peaks of sylvine and arcanite, with more intense sylvine peaks. This observation aligns with the chemical composition, which indicates higher potassium and chlorine levels in energy cane stalk ash. The energy cane leaf ash (V5-L) predominantly displayed peaks of calcite, sylvine, and quartz. Additionally, a significant baseline deviation in the diffractogram suggests the presence of amorphous material.

Although V5-L exhibited less intense quartz peaks compared to SCA-L, it contained higher levels of silicon oxide, as indicated by the chemical composition. This discrepancy can be attributed to the silica in energy cane leaves being predominantly amorphous. Crystalline silicas, such as tridymite and cristobalite, were not detected, indicating that the ash calcination temperature of 600 °C does not induce silica crystallization. Therefore, apart from quartz, the silica present in V5-L is likely reactive silica in an amorphous form.

3.9. Thermal Analyses of the Ash

Figure 10 presents the TG and DTG curves for the ash from (a) sugarcane stalks, (b) sugarcane leaves, (c) energy cane stalks, and (d) energy cane leaves. For both varieties, the stalk ash exhibited an intense downward DTG peak at approximately 120 °C, corresponding to the temperature at which the most significant mass loss occurs. Similarly, leaf ash showed a downward DTG peak near this temperature, but it was less intense and involved less mass loss. This mass loss is attributed to water retained by the ash particles. Although the

ash was dried at 100 °C, it was subsequently stored at room temperature, allowing it to absorb moisture from the air.

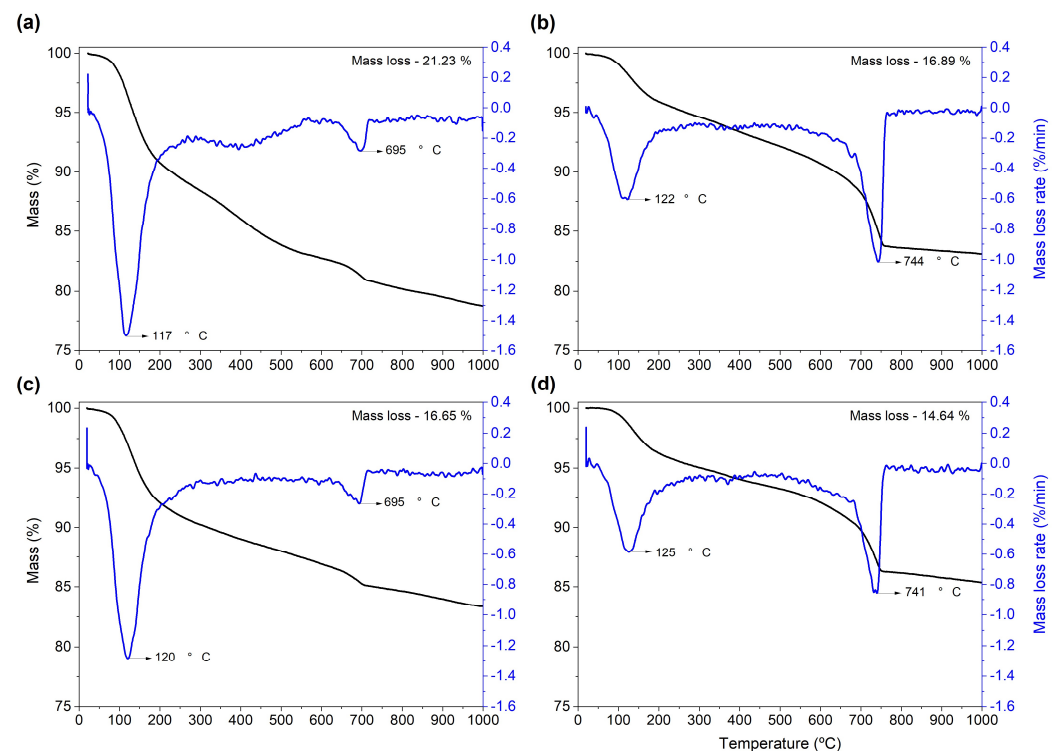


Figure 10. Thermal analysis (TG) and differential thermal analysis (DTG) of (a) SCA-S, (b) SCA-L, (c) V5-S, and (d) V5-L. Temperatures corresponding to DTG main curve peaks have been indicated.

For stalk ash, a less pronounced downward DTG peak was observed at around 695 °C. In contrast, leaf ash exhibited a more intense DTG peak at approximately 740 °C. According to XRD analysis, this process corresponds to the decomposition of calcium carbonate (calcite) present in the leaf ash.

In addition to these two processes—moisture loss and carbonate decomposition—a continuous mass loss was observed between 200 and 400 °C. This behavior aligns with the loss of hydroxyl (OH) groups remaining in the amorphous silica [70].

The thermal analyses of the ashes conducted in this study provide crucial information for their applicability in cementitious systems. The mass loss observed between 200 °C and 400 °C, attributed to the loss of hydroxyl groups from amorphous silica, confirms the presence of reactive material essential for pozzolanic reactions. Additionally, the calcium carbonate decomposition peak identified at temperatures around 740 °C in the leaf ashes reflects the presence of calcite, which can influence the mechanical properties of cementitious composites.

3.10. Compressive Strength of Mortars

Figure 11 shows the compressive strength results for mortars with partial cement replacement by washed pozzolans, tested after 7 and 28 days of curing.

After 7 days, the reference mortar achieved a compressive strength of 32.38 MPa, the highest value among all samples analyzed. The mortars exhibited compressive strengths as percentages of the reference: 94.23% for silica fume, 98.25% for SCA-W-5, 78.77% for SCA-W-10, 85.28% for SCA-W-20, 94.43% for V5-W-5, 89.96% for V5-W-10, and 95.39% for V5-W-20. Despite variations, only the SCA-W-10 mortar showed a statistically significant difference. Thus, with the exception of SCA-W-10, all mortars demonstrated similar strength to the reference after 7 days.

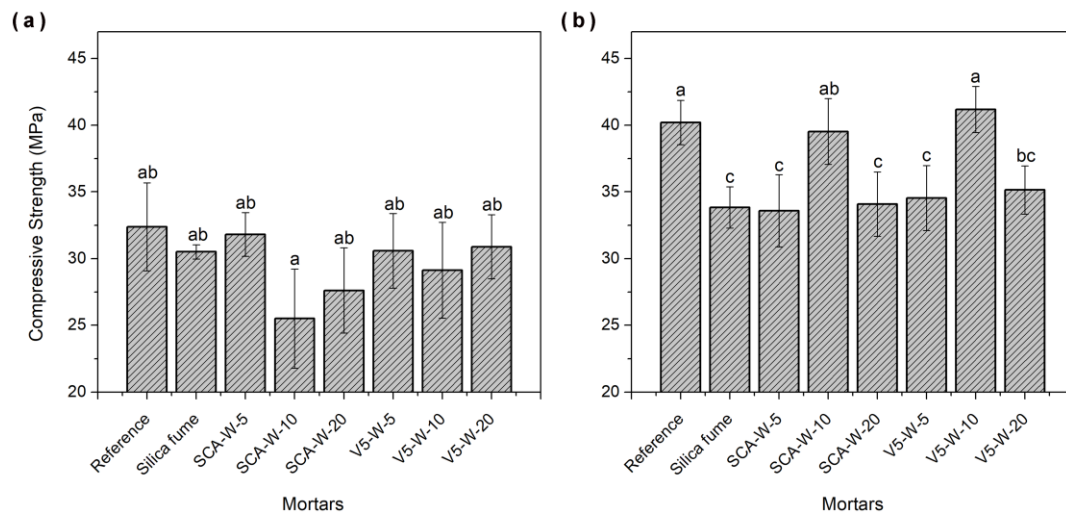


Figure 11. Compressive strength (MPa) of mortars with partial replacement of pozzolan cement after (a) 7 days of curing and (b) 28 days of curing. Means followed by different letters for each mortar (a–c) differ from each other according to the Tukey test at a 5% probability level.

At 28 days, compressive strength values increased, with the reference mortar reaching 40.18 MPa. The lowest values were observed for mortars with silica fume, SCA-W-5, SCA-W-20, and V5-W-5, which showed no statistical differences among them and represented 84.16%, 83.56%, 84.82%, and 85.93% of the reference value, respectively. SCA-W-10 and V5-W-20 achieved 98.34% and 87.46% of the reference value, respectively. The highest compressive strength was observed for the V5-W-10 mortar, representing 102.43% of the reference value, indicating the high reactivity of the V5-W ash. However, no statistical difference was found between V5-W-10 and the reference mortar.

The higher strength observed for 10% replacements suggests that this is the optimal percentage for both sugarcane varieties. This optimal percentage may result from the high reactivity of the ash and the availability of portlandite. For 20% replacement, the reduced availability of portlandite may limit further strength development.

The presented results highlight the suitability of the ashes, particularly those from energy cane leaves, for use as a partial substitute for cement. The high amorphous silica content, corroborated by X-ray diffraction and chemical analysis results, reinforces their ability to react with portlandite released during cement hydration, forming insoluble cementitious compounds and improving the strength of mortars.

From a sustainability perspective, the reuse of ashes as an additive in construction materials not only reduces the need for landfill disposal but also decreases Portland cement consumption, contributing to the mitigation of CO₂ emissions associated with its production. This study provides a solid foundation for exploring application scenarios, such as in the production of sustainable mortars and concretes, with the potential to positively impact the circular economy and reduce industrial waste.

Finally, it is important to emphasize that the use of energy cane ashes in mortars should be accompanied by pre-treatment processes, such as washing, to reduce potassium and chlorine levels to acceptable limits. These steps are essential to minimize negative effects on the properties of cementitious matrices and ensure the durability of the final materials. These results pave the way for future investigations into the mechanical, microstructural, and durability properties of composites utilizing this innovative material.

4. Conclusions

The calcination of energy cane generates approximately four times more ash per hectare compared to sugarcane, emphasizing its potential as a resource for sustainable applications. The microstructural analysis revealed a significantly higher amount of phytoliths in energy cane leaf ash, with dumbbell- and cross-shaped phytoliths oriented longitudinally. The chemical composition showed a higher concentration of SiO₂ in energy cane leaf ash (45.73%), which is 61% greater than sugarcane leaf ash. In stalk ash, both types of cane displayed high levels of potassium, and energy cane stalk ash contained a notable chlorine content.

The compressive strength tests demonstrated that replacing 10% of Portland cement with washed energy cane ash yielded a performance comparable to the reference mortar, achieving 102.43% of its compressive strength after 28 days of curing. This result highlights the excellent pozzolanic reactivity of energy cane ash, particularly when potassium and chlorine are reduced to acceptable levels. Additionally, the potential to repurpose extracted potassium as fertilizer reinforces the circular economy approach, reducing the environmental impact of agricultural and industrial practices.

The findings underscore the suitability of energy cane ash for use in cementitious composites, particularly in scenarios where its high silica content enhances mechanical properties. This study contributes to sustainability by promoting waste valorization, reducing Portland cement consumption, and mitigating CO₂ emissions. Future research should focus on long-term durability and large-scale applications of energy cane ash to further establish its role in advancing sustainable construction practices.

Author Contributions: Conceptualization, G.P.L., L.B., J.R., J.P. and J.A.R.; methodology, G.P.L., L.B., M.V.B., L.S., J.P. and J.R.; validation, G.P.L., M.V.B., L.S., J.P. and J.R.; formal analysis, G.P.L., L.B., M.V.B., L.S., J.P. and J.R.; investigation, G.P.L.; resources, J.P. and J.A.R.; data curation, G.P.L.; writing—original draft preparation, G.P.L.; writing—review and editing, G.P.L., L.B., M.V.B., L.S., J.P. and J.R.; visualization, G.P.L., L.B., M.V.B., L.S., J.P. and J.R.; supervision, J.P. and J.A.R.; project administration, G.P.L., J.P. and J.A.R.; funding acquisition, G.P.L. and J.A.R. All authors have read and agreed to the published version of the manuscript.

Funding: This study was financed in part by the Coordenação de Aperfeiçoamento de Pessoal de Nível Superior—Brasil (CAPES)—Finance Code 001.

Institutional Review Board Statement: Not applicable.

Informed Consent Statement: Not applicable.

Data Availability Statement: The original contributions presented in the study are included in the article; further inquiries can be directed to the corresponding author.

Conflicts of Interest: The authors declare no conflicts of interest.

References

1. Richard, E.P.; Anderson, W.F. Sugarcane, Energy Cane and Napier Grass. In *Cellulosic Energy Cropping Systems*; John Wiley & Sons, Ltd.: Chichester, UK, 2014; pp. 91–108.
2. de Abreu, L.G.F.; Silva, N.V.; Ferrari, A.J.R.; de Carvalho, L.M.; Fiamenghi, M.B.; Carazzolle, M.F.; Fill, T.P.; Pilau, E.J.; Pereira, G.A.G.; Grassi, M.C.B. Metabolite Profiles of Energy Cane and Sugarcane Reveal Different Strategies during the Axillary Bud Outgrowth. *Plant Physiol. Biochem.* **2021**, *167*, 504–516. [[CrossRef](#)] [[PubMed](#)]
3. Viator, R.P.; Richard, E.P. Sugar and Energy Cane Date of Planting Effects on Cane, Sucrose, and Fiber Yields. *Biomass Bioenergy* **2012**, *40*, 82–85. [[CrossRef](#)]
4. Alexander, A.G. *Sugar Cane Physiology: Comprehensive Study of the Saccharum Source-to-Sink System*; Elsevier: Amsterdam, The Netherlands, 1973; ISBN 0444410163.
5. Byrt, C.S.; Grof, C.P.L.; Furbank, R.T. C4 Plants as Biofuel Feedstocks: Optimising Biomass Production and Feedstock Quality from a Lignocellulosic Perspective. *J. Integr. Plant Biol.* **2011**, *53*, 120–135. [[CrossRef](#)] [[PubMed](#)]

6. Matsuoka, S.; Kennedy, A.J.; dos Santos, E.G.D.; Tomazela, A.L.; Rubio, L.C.S. Energy Cane: Its Concept, Development, Characteristics, and Prospects. *Adv. Bot.* **2014**, *2014*, 597275. [CrossRef]
7. FAO. *World Food and Agriculture—Statistical Yearbook 2020*; FAO: Rome, Italy, 2020; ISBN 9789251333945.
8. Companhia Nacional de Abastecimento (CONAB) Produção de Cana-de-Açúcar Na Safra 2023/24 Chega a 713,2 Milhões de Toneladas, a Maior da Série Histórica. Available online: <https://www.conab.gov.br/ultimas-noticias/5489-producao-de-cana-de-acucar-na-safra-2023-24-chega-a-713-2-milhoes-de-toneladas-a-maior-da-serie-historica#:~:text=Nestecen%C3%A1rio,aprodu%C3%A7%C3%A3ototal,delitrosdeetanohidratado> (accessed on 22 August 2024).
9. Setayesh Gar, P.; Suresh, N.; Bindiganavile, V. Sugar Cane Bagasse Ash as a Pozzolan Admixture in Concrete for Resistance to Sustained Elevated Temperatures. *Constr. Build. Mater.* **2017**, *153*, 929–936. [CrossRef]
10. Eggleston, G.; Lima, I. Sustainability Issues and Opportunities in the Sugar and Sugar-Bioprocess Industries. *Sustainability* **2015**, *7*, 12209–12235. [CrossRef]
11. Empresa de Pesquisa Energética (EPE). *National Energy Balance—BEN 2023*; Empresa de Pesquisa Energética (EPE): Rio de Janeiro, Brazil, 2023.
12. Grassi, M.C.B.; Pereira, G.A.G. Energy-Cane and RenovaBio: Brazilian Vectors to Boost the Development of Biofuels. *Ind. Crops Prod.* **2019**, *129*, 201–205. [CrossRef]
13. Pesonen, J.; Kuokkanen, V.; Kuokkanen, T.; Illikainen, M. Co-Granulation of Bio-Ash with Sewage Sludge and Lime for Fertilizer Use. *J. Environ. Chem. Eng.* **2016**, *4*, 4817–4821. [CrossRef]
14. Joshaghani, A.; Moeini, M.A. Evaluating the Effects of Sugar Cane Bagasse Ash (SCBA) and Nanosilica on the Mechanical and Durability Properties of Mortar. *Constr. Build. Mater.* **2017**, *152*, 818–831. [CrossRef]
15. Frías, M.; Villar, E.; Savastano, H. Brazilian Sugar Cane Bagasse Ashes from the Cogeneration Industry as Active Pozzolans for Cement Manufacture. *Cem. Concr. Compos.* **2011**, *33*, 490–496. [CrossRef]
16. Cordeiro, G.C.; Toledo Filho, R.D.; Fairbairn, E.D.M.R. Characterization of Sugar Cane Bagasse Ash for Use as Pozzolan in Cementitious Materials. *Quim. Nova* **2009**, *32*, 82–86. [CrossRef]
17. Matsuoka, S.; Rubio, L.; Santos, E. *The Evolution of Pro-Alcohol*; Agroanalysis: São Paulo, Brazil, 2016; pp. 29–30.
18. Salassi, M.E.; Brown, K.; Hilbun, B.M.; Deliberto, M.A.; Gravois, K.A.; Mark, T.B.; Falconer, L.L. Farm-Scale Cost of Producing Perennial Energy Cane as a Biofuel Feedstock. *Bioenergy Res.* **2014**, *7*, 609–619. [CrossRef]
19. Santchurn, D.; Badaloo, M.G.H.; Zhou, M.; Labuschagne, M.T. Contribution of Sugarcane Crop Wild Relatives in the Creation of Improved Varieties in Mauritius. *Plant Genet. Resour. Characterisation Util.* **2019**, *17*, 151–163. [CrossRef]
20. Shields, S.; Boopathy, R. Ethanol Production from Lignocellulosic Biomass of Energy Cane. *Int. Biodeterior. Biodegrad.* **2011**, *65*, 142–146. [CrossRef]
21. Suhardi, V.S.H.; Prasai, B.; Samaha, D.; Boopathy, R. Evaluation of Pretreatment Methods for Lignocellulosic Ethanol Production from Energy Cane Variety L 79-1002. *Int. Biodeterior. Biodegrad.* **2013**, *85*, 683–687. [CrossRef]
22. Thammasittirong, S.N.R.; Chatwachirawong, P.; Chamduang, T.; Thammasittirong, A. Evaluation of Ethanol Production from Sugar and Lignocellulosic Part of Energy Cane. *Ind. Crops Prod.* **2017**, *108*, 598–603. [CrossRef]
23. Ungureanu, N.; Vlăduț, V.; Biriș, S.-Ș. Sustainable Valorization of Waste and By-Products from Sugarcane Processing. *Sustainability* **2022**, *14*, 11089. [CrossRef]
24. da Silva, J.A. The Importance of the Wild Cane *Saccharum Spontaneum* for Bioenergy Genetic Breeding. *Sugar Tech* **2017**, *19*, 229–240. [CrossRef]
25. Kell, D.B. Breeding Crop Plants with Deep Roots: Their Role in Sustainable Carbon, Nutrient and Water Sequestration. *Ann. Bot.* **2011**, *108*, 407–418. [CrossRef] [PubMed]
26. Carvalho-Netto, O.V.; Bressiani, J.A.; Soriano, H.L.; Fiori, C.S.; Santos, J.M.; Barbosa, G.V.; Xavier, M.A.; Landell, M.G.; Pereira, G.A. The Potential of the Energy Cane as the Main Biomass Crop for the Cellulosic Industry. *Chem. Biol. Technol. Agric.* **2014**, *1*, 20. [CrossRef]
27. de Abreu, L.G.F.; Grassi, M.C.B.; de Carvalho, L.M.; da Silva, J.J.B.; Oliveira, J.V.C.; Bressiani, J.A.; Pereira, G.A.G. Energy Cane vs Sugarcane: Watching the Race in Plant Development. *Ind. Crops Prod.* **2020**, *156*, 112868. [CrossRef]
28. Fanelli, A.; Reinhardt, L.; Matsuoka, S.; Ferraz, A.; da Franca Silva, T.; Hatfield, R.D.; Romanel, E. Biomass Composition of Two New Energy Cane Cultivars Compared with Their Ancestral *Saccharum Spontaneum* during Internode Development. *Biomass Bioenergy* **2020**, *141*, 105696. [CrossRef]
29. Kim, M.; Day, D.F. Composition of Sugar Cane, Energy Cane, and Sweet Sorghum Suitable for Ethanol Production at Louisiana Sugar Mills. *J. Ind. Microbiol. Biotechnol.* **2011**, *38*, 803–807. [CrossRef] [PubMed]
30. Gravois, K.A.; Milligan, S.B. Genetic Relationship between Fiber and Sugarcane Yield Components. *Crop Sci.* **1992**, *32*, 62–687. [CrossRef]
31. Wang, L.; Czedik-Eysenberg, A.; Mertz, R.A.; Si, Y.; Tohge, T.; Nunes-Nesi, A.; Arrivault, S.; Dedow, L.K.; Bryant, D.W.; Zhou, W.; et al. Comparative Analyses of C4 and C3 Photosynthesis in Developing Leaves of Maize and Rice. *Nat. Biotechnol.* **2014**, *32*, 1158–1164. [CrossRef]

32. Matsuoka, S.; Bressiani, J.; Maccheroni, W.; Fouto, I. Sugarcane Bioenergy. In *Sugarcane*; Santos, F., Borém, A., Caldas, C., Eds.; Academic Press: Cambridge, MA, USA, 2012; ISBN 978-85-60249-39-8.
33. Carvalho, V.S.d.; Tannous, K. Thermal Decomposition Kinetics Modeling of Energy Cane *Saccharum Robustum*. *Thermochim. Acta* **2017**, *657*, 56–65. [[CrossRef](#)]
34. Sagastume Gutiérrez, A.; Cabello Eras, J.J.; Huisinigh, D.; Vandecasteele, C.; Hens, L. The Current Potential of Low-Carbon Economy and Biomass-Based Electricity in Cuba. The Case of Sugarcane, Energy Cane and Marabu (*Dichrostachys Cinerea*) as Biomass Sources. *J. Clean. Prod.* **2018**, *172*, 2108–2122. [[CrossRef](#)]
35. Farinha, C.B.; Silvestre, J.D.; de Brito, J.; Veiga, M.d.R. Life Cycle Assessment of Mortars with Incorporation of Industrial Wastes. *Fibers* **2019**, *7*, 59. [[CrossRef](#)]
36. Mehta, P.K. *Pozzolanic and Cementitious By-Products in Concrete—Another Look*; American Concrete Institute: Farmington Hills, MI, USA, 1989.
37. Cordeiro, G.C.; Toledo Filho, R.D.; Fairbairn, E.M.R. Effect of Calcination Temperature on the Pozzolanic Activity of Sugar Cane Bagasse Ash. *Constr. Build. Mater.* **2009**, *23*, 3301–3303. [[CrossRef](#)]
38. Guntzer, F.; Keller, C.; Meunier, J.-D. Benefits of Plant Silicon for Crops: A Review. *Agron. Sustain. Dev.* **2012**, *32*, 201–213. [[CrossRef](#)]
39. Kazmi, S.M.S.; Munir, M.J.; Patnaikuni, I.; Wu, Y.-F. Pozzolanic Reaction of Sugarcane Bagasse Ash and Its Role in Controlling Alkali Silica Reaction. *Constr. Build. Mater.* **2017**, *148*, 231–240. [[CrossRef](#)]
40. Ma, J.F.; Yamaji, N. Silicon Uptake and Accumulation in Higher Plants. *Trends Plant Sci.* **2006**, *11*, 392–397. [[CrossRef](#)] [[PubMed](#)]
41. Piperno, D.R. *Phytoliths: A Comprehensive Guide for Archaeologists and Paleoecologists*; AltaMira P.: Oxford, UK, 2006.
42. Wilding, L.P.; Drees, L.R. Biogenic Opal in Ohio Soils. *Soil Sci. Soc. Am. J.* **1971**, *35*, 1004–1010. [[CrossRef](#)]
43. de Siqueira, A.A.; Cordeiro, G.C. Sustainable Cements Containing Sugarcane Bagasse Ash and Limestone: Effects on Compressive Strength and Acid Attack of Mortar. *Sustainability* **2022**, *14*, 5683. [[CrossRef](#)]
44. Kolawole, J.T.; Babafemi, A.J.; Fanijo, E.; Chandra Paul, S.; Combrinck, R. State-of-the-Art Review on the Use of Sugarcane Bagasse Ash in Cementitious Materials. *Cem. Concr. Compos.* **2021**, *118*, 103975. [[CrossRef](#)]
45. Van Raij, B.; de Andrade, J.C.; Cantarella, H.; Quaggio, J.A. *Chemical Analysis to Evaluate the Fertility of Tropical Soils*; Instituto Agrônomo: Campinas, Brazil, 2001; ISBN 8585564059.
46. Rossi, M. *Pedological Map of the State of São Paulo. Revised and Expanded*; Florestal, I., Ed.; Instituto Florestal: São Paulo, Brazil, 2017; Volume 1, ISBN 978-75-64808-16-4.
47. American Society for Testing and Materials (ASTM). *C114: Standard Test Methods for Chemical Analysis of Hydraulic Cement*; American Society for Testing and Materials (ASTM): West Conshohocken, PA, USA, 2018; p. 33.
48. Lyra, G.P.; Borrachero, M.V.; Soriano, L.; Payá, J.; Rossignolo, J.A. Comparison of Original and Washed Pure Sugar Cane Bagasse Ashes as Supplementary Cementing Materials. *Constr. Build. Mater.* **2021**, *272*, 122001. [[CrossRef](#)]
49. Teixeira, E.R.; Mateus, R.; Camões, A.; Branco, F.G. Quality and Durability Properties and Life-Cycle Assessment of High Volume Biomass Fly Ash Mortar. *Constr. Build. Mater.* **2019**, *197*, 195–207. [[CrossRef](#)]
50. ABNT NBR 5739; Concrete—Compression Test of Cylindrical Specimens. Associação Brasileira de Normas Técnicas: São Paulo, Brazil, 2018; p. 9.
51. Roselló, J.; Soriano, L.; Santamarina, M.P.; Akasaki, J.L.; Melges, J.L.P.; Payá, J. Microscopy Characterization of Silica-Rich Agrowastes to Be Used in Cement Binders: Bamboo and Sugarcane Leaves. *Microsc. Microanal.* **2015**, *21*, 1314–1326. [[CrossRef](#)] [[PubMed](#)]
52. Barber, S.A. *Soil Nutrient Bioavailability: A Mechanistic Approach*, 2nd ed.; Wiley: New York, NY, USA, 1995; ISBN 978-0-471-58747-7.
53. de Andrade, A.F.; Flores, R.A.; Casaroli, D.; Bueno, A.M.; Pessoa-de-Souza, M.A.; de Lima, F.S.R.; Marques, E.P. K Dynamics in the Soil–Plant System for Sugarcane Crops: A Current Field Experiment Under Tropical Conditions. *Sugar Tech* **2021**, *23*, 1247–1257. [[CrossRef](#)]
54. Malavolta, E. *Mineral Nutrition Elements of Plants*; Ceres, A., Ed.; Sociedade Brasileira de Ciência do Solo: São Paulo, Brazil, 1980.
55. International Plant Nutrition Institute. *Agronomic Information on Plant Nutrients*; IPNI: Piracicaba, Brazil, 2020.
56. Watanabe, K.; Fukuzawa, Y.; Kawasaki, S.I.; Ueno, M.; Kawamitsu, Y. Effects of Potassium Chloride and Potassium Sulfate on Sucrose Concentration in Sugarcane Juice Under Pot Conditions. *Sugar Tech* **2016**, *18*, 258–265. [[CrossRef](#)]
57. Diamond, S. A Review of Alkali–Silica Reaction and Expansion Mechanisms 1. Alkalies in Cements and in Concrete Pore Solutions. *Cem. Concr. Res.* **1975**, *5*, 329–345. [[CrossRef](#)]
58. John, V.M.; Cincotto, M.A.; Silva, M.G. Ash and Alternative Binders. In *Tecnologia e Materiais Alternativos de Construção*; Freire, W.J., Beraldo, A.L., Eds.; UNICAMP: Campinas, Brazil, 2003; pp. 145–190.
59. Marschner, P. *Mineral Nutrition of Higher Plants*; Elsevier: Amsterdam, The Netherlands, 2012; ISBN 9780123849052.
60. Jensen, O.M.; Hansen, P.F.; Coats, A.M.; Glasser, F.P. Chloride Ingress in Cement Paste and Mortar. *Cem. Concr. Res.* **1999**, *29*, 1497–1504. [[CrossRef](#)]
61. Mehta, P.K. Durability of Concrete in Marine Environment—A Review. *ACI Symp. Publ.* **1982**, *65*, 1–20.

62. de Castro, A.L.; Pandolfelli, V.C. Review: Concepts of Particle Dispersion and Packing for Special Concretes Production. *Cerâmica* **2009**, *55*, 18–32. [[CrossRef](#)]
63. Havlin, J.L.; Tisdale, S.L.; Nelson, W.L.; Beaton, J.D. *Soil Fertility and Fertilizers*, 8th ed.; Pearson: New York, NY, USA, 2021; ISBN 978-0135033739.
64. Agarie, S.; Hanaoka, N.; Ueno, O.; Miyazaki, A.; Kubota, F.; Agata, W.; Kaufman, P.B. Effects of Silicon on Tolerance to Water Deficit and Heat Stress in Rice Plants (*Oryza sativa* L.), Monitored by Electrolyte Leakage. *Plant Prod. Sci.* **1998**, *1*, 96–103. [[CrossRef](#)]
65. Yoshida, S.; Ohnishi, Y.; Kitagishi, K. Chemical Forms, Mobility and Deposition of Silicon in Rice Plant. *Soil Sci. Plant Nutr.* **1962**, *8*, 15–21. [[CrossRef](#)]
66. Takahashi, E. Uptake Mode and Physiological Functions of Silica. In *Science of Rice Plant Physiology*; Matsuo, T., Kumazawa, K., Ishii, R., Ishihara, K., Hirata, H., Eds.; Nobunkyo: Tokio, Japan, 1995; pp. 420–433.
67. Balasta, M.L.F.C.; Perez, C.M.; Juliano, B.O.; Villareal, C.P.; Lott, J.N.A.; Roxas, D.B. Effects of Silica Level on Some Properties of *Oryza Sativa* Straw and Hull. *Can. J. Bot.* **1989**, *67*, 2356–2363. [[CrossRef](#)]
68. Moraes, J.C.B.; Cordeiro, G.C.; Akasaki, J.L.; Vieira, A.P.; Payá, J. Improving the Reactivity of a Former Ground Sugarcane Bagasse Ash Produced by Autogenous Combustion through Employment of Two Different Additional Grinding Procedures. *Constr. Build. Mater.* **2021**, *270*, 121471. [[CrossRef](#)]
69. ABNT NBR 12653; Pozzolanic Materials—Requirements. Associação Brasileira de Normas Técnicas: São Paulo, Brazil, 2014.
70. Imoisili, P.E.; Ukoba, K.O.; Jen, T.C. Synthesis and Characterization of Amorphous Mesoporous Silica from Palm Kernel Shell Ash. *Bol. La Soc. Esp. Ceram. Y Vidr.* **2020**, *59*, 159–164. [[CrossRef](#)]

Disclaimer/Publisher’s Note: The statements, opinions and data contained in all publications are solely those of the individual author(s) and contributor(s) and not of MDPI and/or the editor(s). MDPI and/or the editor(s) disclaim responsibility for any injury to people or property resulting from any ideas, methods, instructions or products referred to in the content.